HHS Public Access

Author manuscript

Biomaterials. Author manuscript; available in PMC 2020 July 01.

Published in final edited form as:

Biomaterials. 2019 July ; 207: 89–101. doi:10.1016/j.biomaterials.2019.03.015.

Engineering a naturally-derived adhesive and conductive cardiopatch

Brian W. Walker[a], **Roberto Portillo Lara**[b,c], **Chu Yu**[b], **Ehsan Shirzaei Sani**[a], **William Kimball**[b], **Shannon Joyce**[b], and **Nasim Annabi**[a,d,e]

[a]Department of Chemical and Biomolecular Engineering, University of California – Los Angeles, Los Angeles, California 90095, USA.

[b]Department of Chemical Engineering, Northeastern University, Boston, MA, 02115, USA.

[c]Tecnologico de Monterrey, Escuela de Ingeniería y Ciencias, Zapopan, JAL, Mexico.

[d]Biomaterials Innovation Research Center, Brigham and Women's Hospital, Harvard Medical School, Boston, MA, USA.

[e]Center for Minimally Invasive Therapeutics (C-MIT), California NanoSystems Institute (CNSI), University of California - Los Angeles, 570 Westwood Plaza, Los Angeles, CA 90095, USA.

Abstract

Myocardial infarction (MI) leads to a multi-phase reparative process at the site of damaged heart that ultimately results in the formation of non-conductive fibrous scar tissue. Despite the widespread use of electroconductive biomaterials to increase the physiological relevance of bioengineered cardiac tissues *in vitro*, there are still several limitations associated with engineering biocompatible scaffolds with appropriate mechanical properties and electroconductivity for cardiac tissue regeneration. Here, we introduce highly adhesive fibrous scaffolds engineered by electrospinning of gelatin methacryloyl (GelMA) followed by the conjugation of a choline-based bio-ionic liquid (Bio-IL) to develop conductive and adhesive cardiopatches. These GelMA/Bio-IL adhesive patches were optimized to exhibit mechanical and conductive properties similar to the native myocardium. Furthermore, the engineered patches strongly adhered to murine myocardium due to the formation of ionic bonding between the Bio-IL and native tissue, eliminating the need for suturing. Co-cultures of primary cardiomyocytes and cardiac fibroblasts grown on GelMA/Bio-IL patches exhibited comparatively better contractile profiles compared to pristine GelMA controls, as demonstrated by over-expression of the gap junction protein connexin 43. These cardiopatches could be used to provide mechanical support and restore electromechnical coupling at the site of MI to minimize cardiac remodeling and preserve normal cardiac function.

Corresponding author: Dr. Nasim Annabi (nannabi@ucla.edu).

Keywords

GelMA; Bio-ionic Liquid; Electrospinning; Cardiac Patch; Cardiac Tissue Engineering

1. Introduction

Coronary heart disease (CHD) remains one of the major causes of death and disability in developed countries and accounts for approximately one third of all reported deaths in people older than 35 years of age [1]. CHD often leads to partial or complete blockage of a coronary artery due to the rupture of an atherosclerotic plaque, in an event known as myocardial infarction (MI). MI severely restricts blood flow to the myocardium, which causes extensive cardiomyocyte (CM) death [2] and triggers a cascade of remodeling mechanisms such as left ventricle (LV) dilation, myocardium hypertrophy, and the appearance of fibrous and noncontractile scar tissue [3, 4]. Cardiac remodeling has a profound impact on both infarcted and non-infarcted regions of the heart, which greatly impairs normal cardiac function and could lead to chronic heart failure. Moreover, the formation of non-excitable and non-contractile scar tissue leads to asynchronous heart beating, owing to the interruption in the propagation of electrical impulses across the myocardium [5–7]. In recent years, regenerative approaches based on multipotent and pluripotent stem cell therapy have shown great promise both *in vitro* and *in vivo*, albeit with highly heterogeneous outcomes and poor clinical translation [8, 9]. Therefore, significant efforts have been made towards the development of therapeutic strategies that can provide support to the infarcted tissues and restore electromechanical coupling at the site of MI. This in turn could help minimize the formation of scar tissue and thus preserve normal cardiac function.

Cardiac tissue engineering (TE) has enabled the development of temporary biomimetic scaffolds that can promote local cell growth and organization [5]. These scaffolds are mainly aimed at providing mechanical support to the infarcted area, which minimizes cardiac remodeling and helps preserve the contractile function of the heart [10–12]. However, the recapitulation of the morphological and physiological features of the native myocardium remains challenging due to the complexity of structural, biochemical, and biophysical properties of the native cardiac microenvironment [13]. For instance, these scaffolds should exhibit high durability and mechanical resilience to withstand repeated cycles of stretching during cardiac beating [14]. Moreover, the composition of these cardiac patches should be based on biocompatible materials that can also be biodegraded in a clinically relevant time frame. Recent advancements in the field of material chemistry and microfabrication have allowed the engineering of a variety of cell-laden and acellular cardiac patches, which are based on both synthetic and naturally-derived biomaterials [12, 15–20]. However, since electromechanical coupling is essential for the contractile function of the heart, alternative strategies to restore electrical conductivity at the site of MI should also be investigated [21].

Conductive materials have been incorporated into scaffolds to form biomaterials with enhanced electrical properties for cardiac TE applications [22–24]. However, some of the engineered conductive scaffolds formed by using electroconductive polymers (e.g.

polypyrrole (PPy), polyaniline (PANi)) or nanomaterials (e.g. carbon nanotubes (CNTs)) may induce cytotoxicity [25, 26]. Furthermore, conductive nanocomposite hydrogels may experience a reduction in electrical conductivity under deformation due to increased distances between nanoparticles in their network [27]. This may limit their *in vivo* application due to their inability to propagate electrical impulses during contraction and expansion of the cardiac tissues.

Another important design criterion for scaffolds used for cardiac TE is the recapitulation of the fibrillar topography of the native myocardium. This is mainly because major components of the cardiac extracellular matrix (ECM) such as collagen type I and III exist as fibers of varying diameter and length that mediate cell attachment, migration, and spreading [28]. In this regard, a variety of microfabrication techniques have been developed to engineer scaffolds with nano- and microfibrous architectures [29]. Among these, electrospinning is the most commonly used technique to produce fibrillar scaffolds with high surface area to volume ratios, as well as defined spatial density and three-dimensional (3D) orientation [30, 31]. Lastly, although cardiac patches hold great potential for the treatment of MI, their integration with the myocardium by means of sutures or staples may lead to further trauma and blockage of blood supply, bleeding, and infection. While different alternatives such as medical grade cyanoacrylates [32] and other bioadhesives [33–35] have been developed to adhere these patches on the heart, many of these approaches are associated with cytotoxicity and high stiffness (e.g cyanoacrylates), low adhesion and structural stability (e.g. fibrin-based bioadhesives), as well as failure to provide a biomimetic environment that allows for tissue regeneration [12, 36–38]. Therefore, there is an unmet need for engineering highly biocompatible and electroconductive fibrous scaffolds, which can adhere strongly to the myocardium to facilitate biointegration without the need for suturing.

Our group recently introduced a new method to generate highly biocompatible electroconductive hydrogels based on the conjugation of a choline-based bio-ionic liquid (Bio-IL) to different polymers [39]. Here, we aimed to use Bio-IL to develop electroconductive fibrous patches that could adhere strongly to the native myocardium to provide mechanical support and minimize cardiac remodeling following MI. To form these patches, we electrospun the highly biocompatible gelatin methacryloyl (GelMA) prepolymer into fibrous patches that were then chemically conjugated with Bio-IL to impart electroconductivity. We then characterized the physical, mechanical, electroconductive, and tissue adhesive properties of engineered GelMA/Bio-IL patches, as well as their ability to support the growth and function of co-cultures of cardiomyocytes (CMs) and cardiac fibroblasts (CFs) *in vitro*. Lastly, we evaluated the feasibility and safety of *in vivo* suture-free delivery and the cardioprotective effect of GelMA/Bio-IL cardiopatches using a murine model of MI. The intrinsically adhesive and electroconductive fibrous patches could be used to provide support to the infarcted myocardium, while also establishing a cell-supportive microenvironment that restores electromechanical coupling and minimizes cardiac remodeling following MI.

2. Results & Discussion

2.1. Physicochemical characterization of GelMA/Bio-IL cardiopatches.

Fibrous patches were prepared by first electrospinning different concentrations of the GelMA precursor mixed with 1,1,1,3,3,3-hexafluoro-2-propanol (HFIP), onto a static metal collector. Electrospun patches were then incubated in 1.25% (w/v) Irgacure 2959 in ethanol, followed by direct addition of various concentrations of Bio-IL and crosslinking via exposure to UV light for 5 min (Figure 1a). Chemical conjugation of Bio-IL to GelMA was first confirmed via proton nuclear magnetic resonance (^{1}H NMR) as described previously [39]. Briefly, ^{1}H NMR spectra were obtained for Bio-IL, GelMA prepolymer, photocrosslinked GelMA patches, and photocrosslinked GelMA/Bio-IL patches (Figure S1a–d). We then determined the degree of consumption of C=C double bonds in methacryloyl groups during free radical polymerization, which occurred both due to the crosslinking of GelMA and the conjugation of Bio-IL to GelMA. Our results showed that 70.2 ± 7.8% of methacryloyl groups were consumed after photocrosslinking of GelMA/Bio-IL patch, which was significantly higher than those calculated for pure photocrosslinked GelMA patch (56.7 ± 9.1%) (Figure S1e). The larger rate of decay of the C=C double bonds in GelMA/Bio-IL patches represents the chemical conjugation of acrylate groups in Bio-IL to methacryloyl groups in GelMA (Figure S1d).

The native cardiac ECM is comprised of several structural fibrillar proteins such as collagen and elastin, which range from 10 to several hundred nanometers in diameter [40]. The formation of biomimetic fibrous structures plays an important role in the physical characteristics of TE scaffolds, such as their mechanical strength, porosity, and surface area/volume ratio [41]. Hence, we aimed to characterize the fiber topology of GelMA/Bio-IL cardiopatches synthesized with varying concentrations of Bio-IL via scanning electron microscopy (SEM) (Figure 1b–c, and S2). SEM images showed no significant differences in the fiber diameter when different concentrations of Bio-IL were used. The fiber diameter was in the range of 544.0 ± 218.6 nm to 676.7 ± 326.2 nm for the engineered cardiopatches. These results demonstrated that Bio-IL conjugation does not influence fiber diameter, enabling the ability to produce scaffolds with tunable conductivity without varying the microstructures.

2.2. Electroconductive properties of GelMA/Bio-IL cardiopatches.

The conductivity of the engineered patches was analyzed as previously described (Figure S3a) [39]. Our results showed that the conductivity of the scaffolds could be tuned by varying the concentrations of both GelMA and Bio-IL (Figure 1d). For instance, the electrical conductivity of scaffolds fabricated with 10% (w/v) GelMA increased from $0.23 \times 10^{-1} \pm 0.02 \times 10^{-1}$ S/m to $1.38 * 10^{-1} \pm 0.12 \times 10^{-1}$ S/m, and $1.90 \times 10^{-1} \pm 0.18 \times 10^{-1}$ S/m, when the Bio-IL concentration was increased from 33% to 66%, and 100% (v/v), respectively. As expected, GelMA patches fabricated with 0% (v/v) Bio-IL did not demonstrate any conductivity, as GelMA itself is not inherently conductive. On the other hand, patches fabricated with 66% (v/v) Bio-IL exhibited an increase in electrical conductivity from $1.38 \times 10^{-1} \pm 0.13 \times 10^{-1}$ S/m to $1.77 \times 10^{-1} \pm 0.15 \times 10^{-1}$ S/m, and $3.18 \times 10^{-1} \pm 0.01 \times 10^{-1}$ S/m when the GelMA concentration increased from 10% to 12.5%,

and 15% (w/v), respectively. Though GelMA itself is not inherently conductive, this increase in conductivity may be attributed to more functional groups available in the GelMA prepolymer at higher concentration that can react with Bio-IL. Furthermore, these values are within the range of the electrical conductivity of the native myocardium, which has been shown to be between 1.6×10^{-1} S/m (longitudinally) and 0.05×10^{-1} S/m (transversally) [42].

The conductivity of the scaffolds was also characterized after 0, 2, and 4 days of incubation in Dulbecco's phosphate buffered saline (DPBS) at 37 °C to determine the effect of scaffold degradation on electrical conductivity. These results showed that the conductivity of GelMA/Bio-IL cardiopatches exhibited no statistically significant differences after up to 4 days of incubation for all conditions tested (Figure 1e). Furthermore, we also evaluated the conductivity of GelMA/Bio-IL cardiopatches under mechanically strained conditions to determine the effect of scaffold deformation on electrical conductivity. For this, the scaffolds were first dried for 2 h to retain trace amounts of moisture and prevent stiffening. The presence of moisture led to increased conductivity readings as compared to dried samples (Figure 1d), however, allowed samples to be mechanically stretched without breaking. The samples were then stretched at a strain rate of 20% and 40%, and electrical conductivity was measured in the stretched state as described before [39]. Our results showed that there were no statistically significant differences in conductivity of the GelMA/Bio-IL cardiopatches when stretched up to 40% strain, compared to static conditions (Figure S3b). These results demonstrated that the conductivity of the scaffolds remained unaffected following degradation or stretching, which is critical to maintain a consistent supportive microenvironment for the excitable phenotypes that comprise the contractile myocardium. Here, we demonstrated that systematic variations in the formulation of GelMA/Bio-IL cardiopatches yielded scaffolds with a wide range of physicochemical properties. Bio-IL conjugation provided GelMA-based scaffolds with highly tunable electrical conductivity (Figure 1d) without affecting the fiber diameter of the scaffolds (Figure 1b–c). Due to the continuous movement of heart due to beating, we aimed to investigate the conductive properties of these cardiopatches while under mechanical tension, and after up to four days of degradation *in vitro*. Our results showed that the conductive properties of the scaffolds were not affected by the degradation (Figure 1e) or deformation (Figure S3b) of the conductive cardiopatches. Thus, there should not be a significant drop in the conductive properties of our patches while adhered to the heart due to the contraction or expansion of cardiac tissue. Cardiopatches, therefore, should support the electrical pathways of the myocardium by aiding in the propagation of electrical signals throughout all phases of cardiac cycle. This is in contrast to other composite hydrogels fabricated with conductive nanoparticles where the inter-particle distance plays a key role in the conductive properties of the scaffold [27].

2.3. *In vitro* swellability and degradation rates of GelMA/Bio-IL cardiopatches.

Excess water intake could potentially compromise the mechanical and conductive properties of TE scaffolds. Hence, we aimed to evaluate the water uptake capacity of GelMA/Bio-IL cardiopatches. Our results showed that scaffolds fabricated with 10% (w/v) GelMA and varying Bio-IL concentrations swelled rapidly after 4 h of incubation, with no significant

increases in water uptake after 8 and 24 h for all Bio-IL concentrations (Figure 1f). Our results also showed that scaffolds fabricated with 66% and 100% (v/v) Bio-IL underwent significantly higher swelling when compared to scaffolds fabricated with a lower Bio-IL concentration. This behavior could be explained in part due to the presence of hydroxyl (-OH) and amine (-NH2) hydrophilic groups in the Bio-IL structure, which enhances the swelling ratio. There was no statistically significant difference in the swelling ratio of cardiopatches fabricated with 66% and 100% Bio-IL after 8 h. However, we observed a decrease in swelling ratio from 66% to 100% (v/v) Bio-IL concentration after 4 h. This can be explained, in part, due to a higher percentage of Bio-IL that is not conjugated to the GelMA polymer network and is washed out in the first 4 h while submerged in DPBS. Furthermore, scaffolds fabricated with 15% (w/v) GelMA showed a similar trend, with higher swelling ratios obtained at higher concentrations of Bio-IL (Figure S4).

Following implantation, TE scaffolds should biodegrade into nontoxic byproducts to allow the growth of new autologous tissue [43]. Thus, we aimed to characterize the *in vitro* enzymatic degradation profile of GelMA/Bio-IL cardiopatches. Briefly, scaffolds were lyophilized and weighed, followed by incubation in DPBS and 5.0 U/mL of collagenase type II solution at 37 °C for up to 72 h. At the end of this period, the samples were lyophilized and re-weighed to determine the changes in dry mass after degradation. The collagenase solution was replaced daily. Our results showed that the degradation rate increased concomitantly when the Bio-IL concentration was increased for cardiopatches containing 10% (w/v) GelMA (Figure 1g). For example, our results show that following 24 h of incubation in collagenase type II solution, cardiopatches demonstrated a degradation rate of 49.65 ± 11.60% and 71.90 ± 4.55% for scaffolds fabricated with 33% (v/v) and 100% (v/v) Bio-IL, respectively. In addition, we evaluated the *in vitro* degradation profile of our cardiopatches incubated in DPBS solution. Our results showed that after 1 day of incubation, scaffolds fabricated using 10% GelMA and 33% (v/v) Bio-IL exhibited degradation rates corresponding to 25.75% ± 3.57% (Figure S5). At 14 days following incubation, cardiopatches containing 10% (w/v) GelMA and 33% (v/v) Bio-IL exhibited 45.32 ± 4.27% degradation (Figure S5). Moreover, the degradation rate increased concomitantly when the Bio-IL concentration was increased for cardiopatches containing both 10% and 15% (w/v) GelMA. In addition, we did not observe any statistical differences between the degradation rate of the patches fabricated with 10% and 15% (w/v) GelMA after 1 and 14 days. Both degradation studies performed in DPBS as well as in a collagenase solution demonstrated that more rapid degradation occurred in cardiopatches fabricated with a higher concentration of Bio-IL. This trend could be attributed in part to higher amounts of unconjugated Bio-IL that were washed out of the hydrogel network.

2.4. Mechanical characterization of GelMA/Bio-IL cardiopatches.

Scaffolds used for cardiac TE should possess similar mechanical properties to the native myocardium to prevent mechanical mismatches that could impair contractile function of native heart [44, 45]. Thus, we evaluated the mechanical properties of scaffolds fabricated using varying concentrations of GelMA and Bio-IL (Figures 1h and S6a). Our results showed that the engineered patches exhibited highly tunable elastic moduli (i.e., 8.76 ± 0.42 kPa to 145.50 ± 4.10 kPa), which was in the range of the stiffness reported for the native

myocardium (~ 20–100 kPa) [46, 47]. Also, the elastic moduli increased concomitantly with increasing GelMA concentrations (Figure 1h). For instance, the elastic moduli of scaffolds fabricated with 33% (v/v) Bio-IL increased from 19.67 ± 1.70 kPa to 86.23 ± 5.61 kPa, and 110.00 ± 5.56 kPa when the concentration of GelMA increased from 10% to 12.5%, and 15% (w/v), respectively (Figure 1h). Our results also showed that the elastic moduli of the scaffolds could also be increased by increasing the concentration of Bio-IL. For instance, the elastic moduli of scaffolds fabricated with 12.5% (w/v) GelMA increased from 86.23 ± 5.61 kPa to 110.45 ± 9.97 kPa, and 134.06 ± 5.06 kPa when the concentration of Bio-IL was increased from 33% to 66%, and 100% (v/v), respectively (Figure 1h). This increase in mechanical properties of the patches may be due to the electrostatic interactions between the positively charged groups in Bio-IL and the negatively charged functional groups present in the GelMA polymer. Ionic interactions, such as these, have previously been shown to increase mechanical strength in hydrogels [48]. In addition, there might be chemical bonding between the Bio-IL and GelMA prepolymer through photopolymerization, which can also increase the mechanical properties of the patches. Furthermore, the ultimate strain and ultimate stress of the scaffolds were also shown to vary by changing the concentrations of both Bio-IL and GelMA (Figure S6). For instance, the ultimate strain of scaffolds with 10% (w/v) GelMA decreased from 84.2 ± 11.46 kPa to 47.9 ± 8.91 kPa when the concentration of Bio-IL was increased from 33% to 100% (v/v), respectively (Figure S6b). Moreover, the ultimate stress of scaffolds fabricated with 33% (v/v) Bio-IL increased from 31.31 ± 5.18 kPa to 64.59 ± 11.19 kPa, and 89.03 ± 10.41 kPa when the concentration of GelMA was increased from 10% to 12.5%, and 15% (w/v), respectively (Figure S6c). Taken together, these results demonstrated the remarkable mechanical tunability of GelMA/Bio-IL cardiopatches, which is highly advantageous for the engineering of electroconductive scaffolds for a variety of TE and biomedical applications. Our engineered patches did not exhibit any significant increase in their water uptake capacity after 4 h, and up to 24 h of incubation in DPBS (Figure 1f). In addition, our results also showed that the elastic moduli of GelMA/Bio-IL cardiopatches could be tuned by varying the concentration of GelMA and Bio-IL, and that the mechanical properties of the scaffolds were within the range of the native human myocardium (Figure 1h). These characteristics highlight the remarkable potential of GelMA/Bio-IL cardiopatches to be used as cardio-supportive devices, owing to their high electrical conductivity and biocompatibility, controlled swellability and degradability, as well as their biomimetic fibrillar topology and mechanical properties.

2.5. Adhesive properties of GelMA/Bio-IL cardiopatches to physiological tissues.

Biomaterials with strong adhesive properties to wet tissues have emerged as promising strategies for sutureless wound closure following surgical procedures [49]. In this regard, in our previous studies, we demonstrated that GelMA-based hydrogels possess high adhesive strength to various physiological tissues, while also exhibiting superior mechanical performance when compared with commercially available tissue adhesives [37, 50]. Here, we aimed to evaluate the adhesive strength of GelMA/Bio-IL cardiopatches to the native myocardium to determine their potential for sutureless application following MI. We used standard wound closure and burst pressure tests from the American Society for Testing and Materials (ASTM) as well as *ex vivo* experiments using murine cardiac tissue to evaluate the adhesive properties of our engineered cardiopatches. First, wound closure experiments were

carried out to evaluate the adhesive strength of the scaffolds to porcine skin (Figure S7a–b), and murine left ventricular myocardium (Figures 2a–c). Wound closure tests showed that the adhesiveness of GelMA/Bio-IL cardiopatches to porcine skin increased up to 61.97 ± 2.50 kPa by increasing the concentration of Bio-IL (Figure S7b). Furthermore, the adhesive strength of scaffolds synthesized using 66% and 100% (v/v) Bio-IL was shown to be significantly higher than the commercial surgical sealants such Coseal™ (19.4 ± 17.3 kPa) and Evicel® (26.3 ± 4.7 kPa) (Figure S7b). In addition, visual inspection revealed that scaffolds photocrosslinked on the surface of the tissue also adhered strongly to the native murine myocardium (Figure 2a). Similarly, wound closure tests on murine myocardium (Figure 2b) revealed that the adhesiveness of GelMA/Bio-IL cardiopatches increased from 5.1 ± 0.4 to 24.89 ± 2.34 kPa as the Bio-IL concentration enhanced from 0% to 100% (v/v) (Figure 2c). Moreover, the adhesive strength of the engineered GelMA/Bio-IL cardiopatches was significantly higher than other synthesized cardiac sealants such as poloxamine-based hydrogels (~17 kPa) [51], and poly(glycerol sebacate)-co-lactic acid (24 kPa) [52], as well as commercial sealants such as Coseal™ and Evicel®. These results demonstrated that GelMA/Bio-IL cardiopatches can be readily applied to the surface of the myocardium and adhere strongly without the need for sutures or additional tissue adhesives.

We also evaluated the ability of GelMA/Bio-IL cardiopatches to seal tissue defects under applied pressure using collagen sheets based on a standard burst pressure test [37, 38] (Figure S7c–d), as well as *ex vivo* explanted rat hearts (Figures 2d–e). For burst pressure test using collagen sheets, we first created small defects on sections of the tissue, which were then sealed by photocrosslinking the cardiopatch on top of them. We then applied increasing air pressure using a syringe pump connected to a pressure sensor until failure occurred (Figure S7c). Our results showed that the burst pressure of GelMA/Bio-IL cardiopatches adhered onto collagen sheets increased up to 5.36 ± 1.01 kPa by increasing the concentration of Bio-IL (Figure S7d). Moreover, the burst pressure of patches fabricated with 100% (v/v) Bio-IL was significantly higher than the burst pressure of both Coseal™ (1.7 ± 0.1 kPa) and Evicel® (1.5 ± 1.0 kPa) (Figure S7d). We also measured the *ex vivo* burst pressure of explanted rat heart sealed with our adhesive patches fabricated with 10% (w/v) GelMA and varying concentrations of Bio-IL (Figure 2d,e). For the *ex vivo* experiments, after sacrificing the animals, the blood vessels at the base of the heart were sealed with clamps, and a defect was created near the apex, which was then sealed with the patch by applying the GelMA/Bio-IL scaffold and photocrosslinking for 5 min. Our results showed that failure occurred at a pressure of 29.97 ± 5.56 kPa, 32.22 ± 4.38 kPa, and 30.56 ± 4.82 kPa for the heart sealed by the engineered cardiopatch containing 33%, 66%, and 100% (v/v) Bio-IL, respectively. The burst pressure of these cardiopatch formulations were similar to the pressure at failure for the intact heart (i.e., 31.05 ± 0.67 kPa) (Figure 2e). Furthermore, visual inspection revealed that failure did not occur due to detachment or rupture of the adhesive patches for all formulations, but due to bursting of the myocardium distal to the defect (Supplementary video 1). The strong bonding of GelMA/Bio-IL cardiopatches to the myocardium was further confirmed via histological evaluation of the interface between the patch and the tissue (Figure 2f). Hematoxylin and eosin (H&E) stained micrographs revealed a tight interlocking between the scaffold and the myocardium, which further demonstrated the intrinsic ability of the scaffolds to adhere strongly to the native tissue.

Standard wound closure (Figure 2c) and burst pressure (Figure 2e) tests demonstrated the high adhesive strength of the scaffolds, which was superior to commercial tissue adhesives, as well as other proposed bioadhesives, such as a hydrophobic light activated heart glue [53]. These observations were further confirmed via histological evaluation, which revealed the tight interlocking at the interface between the patches and the myocardium (Figure 2f). GelMA has been previously reported as a suitable material to obtain strong adhesion to wet tissues [37]. This is due to the covalent bonds formed between methacrylate groups of GelMA and amine groups of tissue during photocrosslinking [54]. Thus, once photocrosslinking has been completed, the anterior side of our cardiopatches will not adhere to the pericardial sac. In addition, GelMA/Bio-IL cardiopatches demonstrated significantly stronger adhesion to cardiac tissue when fabricated with higher concentrations of Bio-IL. This can be attributed to electrostatic interactions between the negatively charged surface of cardiac tissue (carboxyl group) and our positively charged choline-based Bio-IL [33, 55–57]. In fact, the strong adhesion between GelMA/Bio-IL patches and tissues can be attributed to the formation of two different types of chemical bonds: covalent bonds between GelMA and tissue, and ionic bonds between Bio-IL and tissue (schematic shown in Figure 2f).

Recent studies have also reported the development of adhesive and conductive cardiac patches based on the incorporation of gold-nanorods [12] and dopamine [58] in synthetic polymer networks. While these suture-free strategies greatly enhance the clinical translation of bioengineered cardiopatches by minimizing the risk of additional tissue damage, they may not lead to tissue repair and regeneration due to the absence of cell binding sites in the polymer network. In addition, previous groups have demonstrated the intrinsic potential of GelMA-based scaffolds to act as potent angiogenic niches [59]. Therefore, in contrast to alternative strategies, GelMA/Bio-IL cardiopatches could also act as proangiogenic patches that could help salvage the ischemic myocardium during the early stages following MI [60]. These scaffolds could also be used as a supportive layer that can minimize the risk of free wall rupture during the later stages of cardiac remodeling [61], owing to their strong tissue-adhesiveness biomimetic mechanical properties.

2.6. Evaluation of GelMA/Bio-IL cardiopatches capability to restore impulse propagation across severed striated muscle *ex vivo*.

Electroconductive scaffolds could be used to restore electrical communication between excitable cell types to preserve the functionality of the tissue. Thus, we evaluated the ability of GelMA/Bio-IL cardiopatches to restore impulse propagation between two pieces of skeletal muscle *ex vivo*. For this, the rectus abdominis muscles of Wistar rats were explanted *post-mortem*, cut into square pieces, and placed 3 mm apart from each other on top of the scaffolds (Figure 2g). Pulsed direct current test runs were conducted by applying 50 ms square pulses at increasing frequencies, using short platinum wires that were placed on one of the two samples. Muscle contraction was visually assessed on the opposite sample and the threshold voltage was recorded (Supplementary video 2). As expected, our results showed that scaffolds containing higher concentrations of Bio-IL exhibited comparatively lower threshold voltages as compared to GelMA patches without Bio-IL (Figure 2h). Therefore, the engineered GelMA/Bio-IL cardiopatches could be used to restore the propagation of

electrical impulses and preserve the functionality of excitable tissues damaged by trauma or disease.

2.7. *In vitro* contractile activity and phenotype of CMs cultured on GelMA/Bio-IL cardiopatches.

One of the most important aspects in the design of TE scaffolds is the accurate recapitulation of the different stimuli that modulate cell fate. CMs are electroactive cells that rely on electrical stimuli for maintaining tissue homeostasis and function [62]. Therefore, electroconductive scaffolds hold great potential for cardiac TE since they can promote the propagation of electrical impulses and enhance electromechanical coupling of CMs *in vitro* [63]. Here, we aimed to evaluate the ability of GelMA/Bio-IL cardiopatches to support the growth and the contractile function of co-cultures of freshly-isolated CMs and CFs. For this, primary CMs and CFs (2:1 ratio) were drop seeded on top of GelMA/Bio-IL scaffolds fabricated using different concentrations of Bio-IL. Cell viability and proliferation were evaluated using a commercial Live/Dead assay (Figure 3a) and fluorescent F-actin/cell nuclei staining (Figure 3b), respectively. The results demonstrated that the viability of CMs/CFs remained >90% up to day 7 post-seeding for all conditions tested (Figure 3c). In addition, quantitative analysis of fluorescent images revealed that GelMA/Bio-IL scaffolds support the proliferation of CFs, which led to increasingly higher number of cells throughout the duration of the experiment (Figure S8). The metabolic activity of cells growing on GelMA/Bio-IL cardiopatches was significantly higher than those growing on GelMA controls (Figure 3d). We also evaluated the contractile activity of CMs seeded on GelMA/Bio-IL scaffolds. For this, cell-seeded scaffolds were imaged daily using an inverted microscope equipped with a CCD camera and a temperature-controlled chamber at 37 °C. The beating frequency (beats/min, BPM) of the CMs was calculated from digitized video-recorded sequences using a custom MATLAB program. Our results showed that cells grown on cardiopatches containing 33% and 66% (v/v) Bio-IL exhibited a comparatively more robust contractile behavior, when compared to pristine GelMA and GelMA with 100% (v/v) Bio-IL scaffolds (Figure 3e). Moreover, cells grown on GelMA cardiopatches fabricated with 33% and 66% (v/v) Bio-IL exhibited observable contractility at day 7 post-seeding, and significantly higher beating frequencies (157.143 ± 1.742 BPM and 196.524 ± 1.018 BPM, respectively) than those growing on pristine GelMA patch and GelMA with 100% (v/v) Bio-IL cardiopatches (104.643± 5.845 BPM and 110.210 ± 7.360 BPM, respectively) (Figure 3e). The lower contractile activity of the cells grown on GelMA patches (Supplementary Video 3) can be due to the non-conductivity of the scaffold with no Bio-IL. On the other hand, when 100% (v/v) Bio-IL was used, the excess amount of Bio-IL might cover cell binding sites available on GelMA prepolymer, leading to lower cell attachment and contractile activity (Supplementary Video 5). Highest beating frequency was observed for the cells cultured on cardiopatches with 66% (v/v) Bio-IL (Supplementary Video 4).

The contractile function of the myocardium is established by a complex network of interconnected cells that communicate via gap junction proteins termed connexin, which mediate the propagation of electrical impulses [64]. Here, we evaluated the expression of phenotypic cardiac markers in cells grown on pristine GelMA scaffolds and GelMA cardiopatches containing 66% (v/v) Bio-IL, via immunofluorescent staining (IFS) against

sarcomeric α-actinin (SAA) and connexin 43 (Cxs43). Representative fluorescent images revealed that cells seeded on the scaffolds self-organized in clusters of contracting CMs, which were attached to a layer of CFs proliferating on the surface of the scaffolds (Figure 3f and 3g). Our results also showed that cells grown on GelMA cardiopatches with 66% (v/v) Bio-IL exhibited significantly higher levels of Cxs43 expression, located mainly between the borders of the CFs, as compared to pristine GelMA patches (Figure 3h). These observations suggest that GelMA/Bio-IL cardiopatches could aid in the propagation of electrical impulses between isolated cells to enhance the tissue-level functionality and beating of cardiac constructs.

The native myocardium is an electroactive tissue that can transfer electrical impulses that enable the synchronous contraction of the CMs, which in turn carry out the pump function of the heart. Our results demonstrated that GelMA/Bio-IL cardiopatches could effectively promote the growth and function (Figure 3) of co-cultures of CMs and CFs *in vitro*. Bio-IL conjugation led to a comparatively better contractile profile than pristine GelMA scaffolds, as demonstrated by the increased metabolic activity (Figure 3d) and enhanced beating frequency (Figure 3e) observed for conductive cardiopatches. In the context of cardiac electrophysiology, the propagation of electrical impulses is mediated via connexin proteins such as Cxs43, which enable heterocellular electrical coupling between CMs and CFs [65, 66]. Moreover, previous studies have showed that Cxs43-mediated CF coupling *in vitro* could enable synchronous spontaneous contraction in isolated CMs located up to 300 μm apart [67]. In this regard, IFS (Figure 3f and 3g) showed that CFs growing on conductive scaffolds exhibited significantly higher levels of expression of Cxs43 when compared to GelMA-controls (Figure 3h). Moreover, positive fluorescence against this gap junction protein was mainly located to the borders between the proliferating layer of CFs (Figure 3g). These observations suggested that the conductive properties of GelMA/Bio-IL scaffolds promoted the electromechanical coupling of isolated CMs through the upregulation of Cxs43 in CFs. Furthermore, the disruption of electrical communication between cardiac cells has been shown to contribute to the generation of arrhythmias in fibrotic hearts *in vivo* and hinder the contractile function of TE cardiac constructs [67]. Therefore, Bio-IL conjugation could be used to aid in the rapid propagation of electrical impulses across heterocellular TE scaffolds, and lead to enhanced tissue-level functionality both *in vitro* and *in vivo*.

2.8. *In vivo* application of GelMA/Bio-IL cardiopatches using a murine model of MI.

A series of structural and functional abnormalities occur after the onset of MI, which compromise the contractile function of the heart and could potentially lead to free wall rupture and death [68]. Electrospun fibrous patches have shown great potential to be used as cardio-supportive devices to help minimize the formation of non-contractile scar tissue and thinning of the infarcted myocardium [69, 70]. However, the delivery of conductive scaffolds to the myocardium presents several risks that could potentially lead to impaired cardiac function or fatal arrhythmias [71]. Thus, in this study, we evaluated the feasibility, safety and *in vivo* functionality of GelMA/Bio-IL cardiopatches using a murine model of MI via permanent ligation of the left anterior descending (LAD) coronary artery (Figure 4ai–iv). All infarcts were confirmed via blanching of the myocardium distal to the site of ligation.

Following the induction of MI, animals were divided into three treatment groups: sham, GelMA control, and GelMA/Bio-IL; and followed for a period of 3 weeks to allow for cardiac remodeling. We used scaffolds fabricated with 10% (w/v) GelMA and 33% (v/v) Bio-IL for the treatment group that received conductive cardiopatches. At the end of this period, the animals were sacrificed, and the hearts were excised and processed for histological evaluation using Masson's trichrome and IFS against the cardiac markers SAA and Cxs43. Our results showed strong adhesion of both GelMA (Figure 4b) and GelMA/Bio-IL (Figure 4c) patches to the myocardial tissue after 3 weeks. In addition, tissue ingrowth inside the scaffolds was observed for both GelMA and GelMA/Bio-IL samples. In addition, the cardiopatches were intact on the surface of the myocardium 21 days post implantation. Further, it was found that the sham controls exhibited significant thinning of the myocardium with a large aneurysmal section on the LV (Figure 4di). The infarcted area exhibited a marked reduction in the expression of both SAA and Cxs43, which was indicative of extensive CM death and the appearance of non-contractile scar tissue (Figure 4dii–iii). In contrast, the animals receiving both the GelMA (Figure 4ei) and GelMA/Bio-IL (Figure 4fi) cardiopatches showed comparatively less ventricular wall thinning and no apparent aneurysm at the site of MI after 3 weeks. Furthermore, the expression of phenotypic cardiac markers was maintained throughout the site of MI, which was indicative of the preservation of a fully functional myocardium for both hearts treated with GelMA scaffolds (Figure eii-iii) and GelMA/Bio-IL cardiopatches (Figure 4fii–iii). These results suggested that both GelMA-based patches could establish a cell-supportive microenvironment that prevented the remodeling of the myocardium at the site of MI and preserve normal tissue architecture. Furthermore, the expression of characteristic phenotypic markers SAA and Cxs43 was indicative of the preservation of viable myocardium and the maintenance of normal cardiac function.

Following MI, cardiac remodeling triggers a series of molecular and cellular changes that manifest clinically as changes in ventricular wall thickness and the appearance of fibrotic scar tissue [61]. In recent years, electrospun scaffolds have shown great potential to be used as cardio-supportive devices, which can help minimize the formation of non-contractile scar tissue and thinning of the ventricular wall following MI [70]. Here, we evaluated the feasibility and safety of *in vivo* delivery as well as the cardioprotective potential of GelMA/Bio-IL cardiopatches using a murine model of MI via permanent LAD ligation (Figure 4ai–iv). Histological evaluation revealed that the hearts treated with both GelMA and GelMA/Bio-IL patches exhibited minimal tissue remodeling and LV wall thinning, when compared to untreated animals (Figure 4d–f). These observations suggested that the supportive function of both GelMA and GelMA/Bio-IL scaffolds could potentially ameliorate LV wall stress and preserve normal tissue architecture. These results were in accordance to previous studies showing that cardio-supportive devices with ECM-like properties can mediate endogenous repair mechanisms to improve heart function [72]. Moreover, these studies also showed that the attenuation of pathological cardiac remodeling occurred mainly due to architectural and compositional cues that potentiated tissue regeneration, independent of scaffold electroconductivity.

Our results suggested that GelMA/Bio-IL scaffolds yielded tissue constructs with comparatively better *in vitro* functionality, which could be due in part to enhanced

electromechanical coupling via upregulation of the gap junction protein Cxs43. Moreover, *in vivo* evaluation showed that both conductive and non-conductive GelMA-based scaffolds led to the preservation of normal tissue architecture by minimizing cardiac remodeling after MI. These observations could be explained in part due to the complex interplay of different bioactive cues that are normally present *in vivo* [73–76], which were not replicated in our experiments *in vitro*. Furthermore, these results demonstrated that cardiac remodeling could be effectively prevented using acellular scaffolds without the need for exogenous cytokines or growth factors, which is highly advantageous for the clinical translation of these scaffolds. For instance, Montgomery *et al.* recently reported a microfabricated injectable scaffold that could be used to deliver viable and functional CMs to the site of MI [77]. Although the scaffolds could be delivered through a minimally invasive procedure and significantly improved cardiac function following MI, both adult and stem cell-based strategies for the treatment of MI often shown highly heterogenous outcomes and poor clinical translation [8, 9]. Moreover, one of the most relevant characteristics of GelMA/Bio-IL cardiopatches was their high adhesive strength to the beating myocardium after photocrosslinking, even in the presence of blood (Figure 4aiii–iv). Recently, Lang *et al.* reported the development of blood-resistant and light-activated surgical glue that could be used to seal cardiac wall defects in large animal models [78]. Although this bioadhesive could be used by itself to form an on-demand hemostatic seal or in combination with a patch, GelMA/Bio-IL cardiopatches attached strongly to the native tissue without the need for additional adhesives or sutures. This also allowed the establishment of a tight interface and enhance the interlocking between GelMA and collagen fibers from the ECM-like fibrous patch and the myocardium, respectively, which is characteristic of strong tissue adhesives [34, 79]. In addition, cardiopatches photocrosslinked on the surface of rat hearts did not exhibit significant changes in size due to water uptake of the scaffolds (Figure 4aiii–iv). This demonstrates that swelling of our engineered cardiopatches would not significantly compress cardiac tissues *in vivo*.

In situ photocrosslinking of cardiopatches on the beating heart could possibly lead to systemic dissemination of unreacted components and thus, trigger toxic or inflammatory responses that could not be evaluated *in vitro*. Our preliminary *in vivo* experiments confirmed that our electroconductive patches could be safely administered on the myocardium via *in situ* photopolymerization and did not induce any cytotoxicity. In addition, the heart is a highly dynamic organ and the presence of blood and other fluids, as well as cardiac beating could greatly impair the adherence of the patches to the myocardium *in vivo*. Our *in vivo* results here demonstrated that the engineered patches exhibited high adhesion to the native murine myocardium without the need for suturing. Lastly, although the electroconductive and mechanical properties of the patches were tuned to mimic the native tissue, the delivery of a scaffold with these features to the myocardium could potentially impair cardiac function or even lead to fatal arrhythmias. Therefore, our current study aimed on evaluating the safety of *in vivo* delivery of Bio-IL functionalized patches before assessing the therapeutic effects of this strategy. Our future study will focus on evaluating heart function after applying the electroconductive patches using echocardiography, as well as studying the molecular and cellular mechanisms that could be selectively triggered by the delivery of an electroconductive scaffold to the site of MI.

3. Conclusion

In this work, we introduced a new class of adhesive and electroconductive cardiopatches for the treatment of MI. Cardiopatches were synthesized from two naturally derived sources: GelMA, and a highly electroconductive and biocompatible choline-based Bio-IL. The mechanical and conductive properties of these cardiopatches were shown to be readily tunable by varying the concentrations of GelMA and Bio-IL. Bio-IL functionalization rendered cardiopatches with high adhesive strength to the native myocardium, which was comparatively superior to commercially available adhesives, such as Coseal™ and Evicel®. GelMA/Bio-IL cardiopatches could support the growth and function of primary CMs and CFs seeded on the surface of the scaffolds in vitro. Our results showed that electroconductive scaffolds exhibited comparatively better contractile profiles than pristine controls due to the overexpression of the gap junction protein Cxn43. GelMA/Bio-IL cardiopatches could be readily attached to the epicardial surface of the heart via photocrosslinking, which eliminates the need for sutures that could lead to further tissue trauma. Furthermore, histological assessment was indicative of comparatively lower thinning of the ventricular wall 3 weeks after induction of experimental MI. However, further experiments focusing on the evaluation of cardiac function following MI are needed to elucidate the cardioprotective efficacy of this strategy. In addition, the long-term effects of the epicardial application of the cardiopatches and the potential development of co-morbidities such as constrictive pericarditis, arrhythmias and other systemic syndromes should also be evaluated. GelMA/Bio-IL cardiopatches hold great potential to be used as scaffolds to provide mechanical stabilization to the injured myocardium and to restore electromechanical coupling at the site of MI.

4. Experimental Section

4.1. Cardiopatch Fabrication:

Porcine GelMA was synthesized as described previously [80]. A prepolymer solution was then prepared by mixing 10, 12.5, and 15% (w/v) of GelMA in hexafluoroisopropanol (HFIP) (Sigma-Aldrich), and placed in a syringe with a 27G needle. The prepolymer solution was then pumped out of the syringe at a rate of 1 mL/h. A high voltage power source (Glassman High Voltage, Inc., Series EH) was attached to the needle of the syringe, and to a metal collector that the GelMA polymer was drawn to, creating a fibrous mat. Fibrous scaffolds were then removed from the collector plate and placed in a vacuum to remove any remaining solvent. Scaffolds were then placed in a solution bath containing 1.25% (w/v) photoinitiator Irgacure 2959 (Sigma-Aldrich) in ethanol. Bio-IL was also synthesized using the previously discussed methodology [39]. Four concentrations of Bio-IL in water were prepared including 0, 33, 66, and 100% (v/v). Scaffolds were placed in a refrigerator to prevent the dissolving of GelMA fibers in Bio-IL/water solution. A volume of 1 mL Bio-IL was then placed on the surface of GelMA fibrous scaffolds and immediately crosslinked using UV irradiation for 300 s on each side of the scaffold.

4.2. ^{1}H NMR Characterization:

^{1}H NMR analysis was performed using a Varian Inova-500 NMR spectrometer. ^{1}H NMR spectra were obtained for a choline-based Bio-IL prepolymer, GelMA, prepolymer, GelMA

fibers after UV photocrosslinking, and Bio-IL/GelMA cardiopatches. Methacrylated groups were identified due to the presence of peak values at δ = 5.3. and 5.7 ppm. The decreasing rate for the C=C double bond signals $\left(-\frac{\partial(C=C)}{\partial t}\right)$ in methacrylate group of GelMA was associated with the extent of crosslinking of cardiopatch, as well as conjugation of GelMA to Bio-IL. This area decrease was calculated using the following equation:

$$\text{Decay of methacrylate group}(\%) = \left(\frac{PA_b - PA_a}{PA_b}\right) \times 100\%$$

where PA_b, and PA_a represent the peak areas of methacrylated groups before and after photocrosslinking, respectively. Accordingly, PA_b - PA_a corresponds to the concentration of methacrylated groups consumed in the photocrosslinking process. ACD/Spectrus NMR analysis software were used to integrate the area under the peaks and all the data was analyzed with respect to phenyl group peaks at δ = 6.5–7.5 ppm.

4.3. Scanning Electron Microscopy (SEM) Analysis:

The diameter and morphology of the electrospun nanofibrous sheets were examined by SEM; Hitachi S-4800, Japan. Prior to imaging, the samples were fixed in 2% osmium tetroxide (OsO_4, Fisher Scientific). The scaffolds were then washed three times with DPBS each for 5 min, followed by dehydration in graded ethanol series (i.e., 30, 50, 70, 95, and 100% v/v) each for 10 min. Next, samples were dried at critical point with a Tousimis critical point dryer. After drying, the scaffolds were sputter coated with gold/palladium (6 μm). The obtained images were processed by ImageJ software to determine the average fiber diameter sizes (50 arbitrary fibers per each group).

4.4. *In Vitro* Evaluation of Conductivity:

Cardiopatches were photocrosslinked with UV irradiation for 300 s on each side and allowed to dry for 24 h. Once dried, conductivity analysis was performed using a two-probe electrical station connected to a Semiconductor Parameter analyzer, as previously described (Figure S3a) [81]. The results were then analyzed to determine the electrical conductivity of cardiopatches. Cardiopatches were also examined for conductivity following degradation in DPBS at 37 °C for a period of 0, 2, and 4 d. Samples were removed from DPBS and allowed to dry for 24 h. Electrical conductivity was then measured using the same protocol to measure electrical conductivity in samples that had not degraded. The conductivity of cardiopatches was also determined using methods previously described [81]. Cardiopatches were also examined for conductivity under stretched conditions. Briefly, cardiopatches were fabricated using the same method as above, but were dried for only 2 h to prevent brittleness. The trace amount of moisture led to increased conductivity readings, however, allowed samples to be mechanically stretched without breaking. Samples were stretched at a strain of 0, 20, and 40% and conductivity was measured using the same method as above. At least 5 samples were tested for each condition.

4.5. Swelling Ratio Measurements:

Cardiopatches of varying GelMA and Bio-IL concentrations were synthesized as described previously and cut into small pieces. The small pieces were then lyophilized, weighed, and placed in DPBS at 37 °C. At prearranged time points (4, 8, 24 h), samples were removed and weighed again after immersion. The swelling of the samples was calculated as the ratio of the swelled mass to the mass of the lyophilized sample.

4.6. *In Vitro* Degradation Test:

Cardiopatches were synthesized as previously described, cut into small square sections, and lyophilized overnight. Samples were weighed and placed in 1.5 mL tubes of 1 mL DPBS with 5.0 U/mL collagenase type II, and incubated at 37 °C for up to 72 h. The collagenase solution was refreshed every 24 h. At prearranged points (after 6, 12, 24, 48, and 72 h), the collagenase solution was removed, and samples were lyophilized for 24 h and weighed. The percentage of degradation (D %) of the cardiac patches was calculated using the below equation:

$$D\% = \frac{W_i - W_t}{W_i} \times 100\%$$

where W_i is the initial dry weight of the patch, and W_t is the dry weight after time t.

4.7. Mechanical Testing:

Tensile test was performed on cardiac patches using an Instron 5944 mechanical tester using method previously described [81]. At least 5 samples were tested for each condition.

4.8. Wound Closure Test:

Wound closure tests were performed using a modified ASTM F2458–05 to determine the adhesive strength based on the previously explained procedures [38, 50, 82]. Porcine skin and rat myocardium wet tissues were used as substrates. Briefly, samples of the biological substrate were cut into 40 × 20 mm pieces with a thickness of approximately 5 mm. The substrate was immersed in DPBS to prevent drying. Tissue samples were then glued with cyanoacrylate adhesive onto glass slides. Two sections of the substrate were then placed against each other, and a cardiopatch was photocrosslinked for 300 s over the tissues to glue them together. An Instron mechanical tester was used to measure the maximum adhesive strength at the point of patch failure.

4.9. Burst Pressure Test:

Burst pressure adhesion test was performed using a modified ASTM F2392–04 for determining the sealing strength of a biomaterial. Collagen sheets were used as substrates. First, the collagen sheet was soaked in DPBS for 1 h and placed between two Teflon plates and placed into a custom-designed burst pressure apparatus. A 3 mm defect was then created into the substrate using a surgical blade. Cardiopatches were then fabricated and photocrosslinked on the defect site, and air pressure was increased until patch failure (Figure S7c).

A modified *ex vivo* burst pressure test was conducted using cardiopatches photocrosslinked on freshly explanted rat hearts according to previously published reports [33]. Briefly, an air tube was fed through the top of excised rat hearts into the LV, and a defect was created on the myocardial wall of the LV using a surgical blade (2 mm). Cardiopatches were photocrosslinked onto the defect site. Rat hearts were then placed in a beaker containing water and air pressure was increased in the LV until patch failure.

4.10. *Ex Vivo* Evaluation of Electrical Conductivity:

Adult female Wistar rats were provided by the Institutional Animal Care and Use Committee (ICAUC) at Northeastern University (Boston, MA, USA). All experiments were performed in accordance with relevant guidelines and regulations. Immediately after euthanasia, the rectus abdominus tissue was removed from Wistar rats and placed in DPBS. The rectus abdominus was cut into small square pieces and placed adjacently with a 3 mm gap on cardiopatches with varying Bio-IL concentration. 50 ms square pulses of direct current were applied to the tissue using an Agilent wave generator (Agilent 33220A). The electrical stimulation was applied to one piece of abdominal tissue using short platinum wires with 0.25 mm diameter and 99.9% trace metal basis, bought from Sigma-Aldrich (MO, USA). The threshold was measured by increasing voltage applied to one section of abdominal tissue and observing the lowest voltage at which the neighboring section of tissue contracted.

4.11. Surface Seeding of Primary CMs and CFs on GelMA/Bio-IL Cardiopatches:

A thin layer of 10% (w/v) GelMA was electrospun onto 0.8 × 0.8 cm glass slides, coated with 3-(trimethoxysilyl) propyl methacrylate (TMSPMA). The glass slides were then soaked in 1.25% (w/v) Irgacure 2959 solution for 1 h, and kept at −80 °C for 1 min. A conductive layer was then formed on top of the electrospun GelMA by pipetting a 50-μl drop of Bio-IL at different concentrations (i.e., 0%, 33%, 66%, and 100% (v/v)), followed by UV-initiated photocrosslinking for 5 min. The samples were incubated overnight in Dulbecco's Modified Eagle Medium (DMEM) supplemented with 10% Nu-Serum growth supplement, and 1% penicillin/streptomycin. Primary CMs and CFs were isolated from neonatal rat hearts as described previously [39]. Co-cultures of CMs/CFs were then seeded at a ratio of 2:1 on top of the scaffolds at a density of 2×10^5 cells/cm^2 and maintained at 37 °C, in a 5% CO_2 humidified atmosphere for up to 7 days. Cell viability, and metabolic activity were determined at days 1, 4, and 7 post-seeding as described in our previous publication [39]. IFS against cardiac markers SAA and Cxs43 was carried out as described previously [39].

4.12. *In Vivo* Evaluation of Biosafety and Cardioprotective Potential of Electrospun Scaffolds:

All experiments were performed according to the protocol approved by the IACUC at Northeastern University. Experimental MI was induced via permanent ligation of the LAD as described previously [83]. Immediately after induction of MI, the scaffolds were delivered to the surface of the left ventricle, distal to the site of MI, and photocrosslinked for 300 s using UV light. To remove any unreacted Bio-IL, saline was pipetted to the surface of cardiopatches and excess liquid was collected using a gauze pad. Animals were divided into three groups: sham (control), pristine GelMA patches (i.e., 10% (w/v) GelMA), and GelMA/

Bio-IL patches (i.e., 33% (v/v) Bio-IL and 10% (w/v) GelMA). There were 3 animals per group. Following administration of the treatments, the animals were allowed to recover after anatomical wound closure and followed for a period of 3 weeks. After this period, the animals were euthanized, and the hearts were removed and processed for histological evaluation and IFS as described previously [39].

Supplementary Material

Refer to Web version on PubMed Central for supplementary material.

Acknowledgements

The authors acknowledge the support from the American Heart Association (AHA, 16DG31280010) and the National Institutes of Health (R01-EB023052; R01HL140618).

References

[1]. Sanchis-Gomar F, Perez-Quilis C, Leischik R, Lucia A, Epidemiology of coronary heart disease and acute coronary syndrome, Ann Transl Med 4(13) (2016) 256. [PubMed: 27500157]

[2]. Reis LA, Chiu LL, Feric N, Fu L, Radisic M, Biomaterials in myocardial tissue engineering, J Tissue Eng Regen Med 10(1) (2016) 11–28. [PubMed: 25066525]

[3]. Sutton MG, Sharpe N, Left ventricular remodeling after myocardial infarction: pathophysiology and therapy, Circulation 101(25) (2000) 2981–8. [PubMed: 10869273]

[4]. Westman PC, Lipinski MJ, Luger D, Waksman R, Bonow RO, Wu E, Epstein SE, Inflammation as a Driver of Adverse Left Ventricular Remodeling After Acute Myocardial Infarction, J Am Coll Cardiol 67(17) (2016) 2050–60. [PubMed: 27126533]

[5]. Kai D, Prabhakaran MP, Jin G, Ramakrishna S, Polypyrrole-contained electrospun conductive nanofibrous membranes for cardiac tissue engineering, J Biomed Mater Res A 99(3) (2011) 376–85. [PubMed: 22021185]

[6]. Pfeffer MA, Braunwald E, Ventricular remodeling after myocardial infarction. Experimental observations and clinical implications, Circulation 81(4) (1990) 1161–72. [PubMed: 2138525]

[7]. Talman V, Ruskoaho H, Cardiac fibrosis in myocardial infarction-from repair and remodeling to regeneration, Cell Tissue Res 365(3) (2016) 563–81. [PubMed: 27324127]

[8]. Cambria E, Steiger J, Gunter J, Bopp A, Wolint P, Hoerstrup SP, Emmert MY, Cardiac Regenerative Medicine: The Potential of a New Generation of Stem Cells, Transfus Med Hemother 43(4) (2016) 275–281. [PubMed: 27721703]

[9]. Le TY, Thavapalachandran S, Kizana E, Chong JJ, New Developments in Cardiac Regeneration, Heart Lung Circ 26(4) (2017) 316–322. [PubMed: 27916592]

[10]. Rai R, Tallawi M, Frati C, Falco A, Gervasi A, Quaini F, Roether JA, Hochburger T, Schubert DW, Seik L, Barbani N, Lazzeri L, Rosellini E, Boccaccini AR, Bioactive electrospun fibers of poly(glycerol sebacate) and poly(epsilon-caprolactone) for cardiac patch application, Adv Healthc Mater 4(13) (2015) 2012–25. [PubMed: 26270628]

[11]. Chen Q-Z, Harding SE, Ali NN, Lyon AR, Boccaccini AR, Biomaterials in cardiac tissue engineering: Ten years of research survey, Materials Science and Engineering: R: Reports 59(1) (2008) 1–37.

[12]. Malki M, Fleischer S, Shapira A, Dvir T, Gold Nanorod-Based Engineered Cardiac Patch for Suture-Free Engraftment by Near IR, Nano Lett (2018).

[13]. Atmanli A, Domian IJ, Recreating the Cardiac Microenvironment in Pluripotent Stem Cell Models of Human Physiology and Disease, Trends Cell Biol 27(5) (2017) 352–364. [PubMed: 28007424]

[14]. Huyer LD, Montgomery M, Zhao Y, Xiao Y, Conant G, Korolj A, Radisic M, Biomaterial based cardiac tissue engineering and its applications, Biomed Mater 10(3) (2015) 034004. [PubMed: 25989939]

[15]. Izadifar M, Chapman D, Babyn P, Chen X, Kelly ME, UV-Assisted 3D Bioprinting of Nanoreinforced Hybrid Cardiac Patch for Myocardial Tissue Engineering, Tissue Eng Part C Methods 24(2) (2018) 74–88. [PubMed: 29050528]

[16]. Schaefer JA, Guzman PA, Riemenschneider SB, Kamp TJ, Tranquillo RT, A cardiac patch from aligned microvessel and cardiomyocyte patches, J Tissue Eng Regen Med 12(2) (2018) 546–556. [PubMed: 28875579]

[17]. Wang QL, Wang HJ, Li ZH, Wang YL, Wu XP, Tan YZ, Mesenchymal stem cell-loaded cardiac patch promotes epicardial activation and repair of the infarcted myocardium, J Cell Mol Med 21(9) (2017) 1751–1766. [PubMed: 28244640]

[18]. Tang J, Vandergriff A, Wang Z, Hensley MT, Cores J, Allen TA, Dinh PU, Zhang J, Caranasos TG, Cheng K, A Regenerative Cardiac Patch Formed by Spray Painting of Biomaterials onto the Heart, Tissue Eng Part C Methods 23(3) (2017) 146–155. [PubMed: 28068869]

[19]. Sugiura T, Hibino N, Breuer CK, Shinoka T, Tissue-engineered cardiac patch seeded with human induced pluripotent stem cell derived cardiomyocytes promoted the regeneration of host cardiomyocytes in a rat model, J Cardiothorac Surg 11(1) (2016) 163. [PubMed: 27906085]

[20]. Tallawi M, Dippold D, Rai R, D'Atri D, Roether JA, Schubert DW, Rosellini E, Engel FB, Boccaccini AR, Novel PGS/PCL electrospun fiber mats with patterned topographical features for cardiac patch applications, Mater Sci Eng C Mater Biol Appl 69 (2016) 569–76. [PubMed: 27612749]

[21]. Monteiro LM, Vasques-Novoa F, Ferreira L, Pinto-do OP, Nascimento DS, Restoring heart function and electrical integrity: closing the circuit, NPJ Regen Med 2 (2017) 9. [PubMed: 29302345]

[22]. Li X, Zhao T, Sun L, Aifantis KE, Fan Y, Feng Q, Cui F, Watari F, The applications of conductive nanomaterials in the biomedical field, J Biomed Mater Res A 104(1) (2016) 322–39. [PubMed: 26179845]

[23]. Balint R, Cassidy NJ, Cartmell SH, Conductive polymers: towards a smart biomaterial for tissue engineering, Acta Biomater 10(6) (2014) 2341–53. [PubMed: 24556448]

[24]. Shi Z, Gao X, Ullah MW, Li S, Wang Q, Yang G, Electroconductive natural polymer-based hydrogels, Biomaterials 111 (2016) 40–54. [PubMed: 27721086]

[25]. Vashist A, Kaushik A, Vashist A, Sagar V, Ghosal A, Gupta YK, Ahmad S, Nair M, Advances in Carbon Nanotubes-Hydrogel Hybrids in Nanomedicine for Therapeutics, Adv Healthc Mater 7(9) (2018) e1701213. [PubMed: 29388356]

[26]. Pok S, Vitale F, Eichmann SL, Benavides OM, Pasquali M, Jacot JG, Biocompatible carbon nanotube-chitosan scaffold matching the electrical conductivity of the heart, Acs Nano 8(10) (2014) 9822–32. [PubMed: 25233037]

[27]. Thoniyot P, Tan MJ, Karim AA, Young DJ, Loh XJ, Nanoparticle-Hydrogel Composites: Concept, Design, and Applications of These Promising, Multi-Functional Materials, Adv Sci (Weinh) 2(1–2) (2015) 1400010. [PubMed: 27980900]

[28]. Qu B, Chen C, Qian L, Xiao H, He B, Facile preparation of conductive composite hydrogels based on sodium alginate and graphite, Mater Lett 137 (2014).

[29]. Zhang B, Xiao Y, Hsieh A, Thavandiran N, Radisic M, Micro- and nanotechnology in cardiovascular tissue engineering, Nanotechnology 22(49) (2011) 494003. [PubMed: 22101261]

[30]. Kitsara M, Agbulut O, Kontziampasis D, Chen Y, Menasche P, Fibers for hearts: A critical review on electrospinning for cardiac tissue engineering, Acta Biomater 48 (2017) 20–40. [PubMed: 27826001]

[31]. Ehler E, Jayasinghe SN, Cell electrospinning cardiac patches for tissue engineering the heart, Analyst 139(18) (2014) 4449–52. [PubMed: 25058315]

[32]. Lee Y, Xu C, Sebastin M, Lee A, Holwell N, Xu C, Miranda Nieves D, Mu L, Langer RS, Lin C, Karp JM, Bioinspired Nanoparticulate Medical Glues for Minimally Invasive Tissue Repair, Adv Healthc Mater 4(16) (2015) 2587–96. [PubMed: 26227833]

[33]. Li J, Celiz AD, Yang J, Yang Q, Wamala I, Whyte W, Seo BR, Vasilyev NV, Vlassak JJ, Suo Z, Mooney DJ, Tough adhesives for diverse wet surfaces, Science 357(6349) (2017) 378–381. [PubMed: 28751604]

[34]. Mahdavi A, Ferreira L, Sundback C, Nichol JW, Chan EP, Carter DJ, Bettinger CJ, Patanavanich S, Chignozha L, Ben-Joseph E, Galakatos A, Pryor H, Pomerantseva I, Masiakos PT, Faquin W, Zumbuehl A, Hong S, Borenstein J, Vacanti J, Langer R, Karp JM, A biodegradable and biocompatible gecko-inspired tissue adhesive, Proc Natl Acad Sci U S A 105(7) (2008) 2307–12. [PubMed: 18287082]

[35]. Pandey N, Hakamivala A, Xu CC, Hariharan P, Radionov B, Huang Z, Liao J, Tang LP, Zimmern P, Nguyen KT, Hong Y, Biodegradable Nanoparticles Enhanced Adhesiveness of Mussel-Like Hydrogels at Tissue Interface, Advanced Healthcare Materials 7(7) (2018).

[36]. Suh M, Proctor D, Chappell G, Rager J, Thompson C, Borghoff S, Finch L, Ellis Hutchings R, Wiench K, A review of the genotoxic, mutagenic, and carcinogenic potentials of several lower acrylates, Toxicology 402–403 (2018) 50–67.

[37]. Assmann A, Vegh A, Ghasemi-Rad M, Bagherifard S, Cheng G, Sani ES, Ruiz-Esparza GU, Noshadi I, Lassaletta AD, Gangadharan S, Tamayol A, Khademhosseini A, Annabi N, A highly adhesive and naturally derived sealant, Biomaterials 140 (2017) 115–127. [PubMed: 28646685]

[38]. Annabi N, Zhang YN, Assmann A, Sani ES, Cheng G, Lassaletta AD, Vegh A, Dehghani B, Ruiz-Esparza GU, Wang X, Gangadharan S, Weiss AS, Khademhosseini A, Engineering a highly elastic human protein-based sealant for surgical applications, Sci Transl Med 9(410) (2017).

[39]. Noshadi I, Walker BW, Portillo-Lara R, Shirzaei Sani E, Gomes N, Aziziyan MR, Annabi N, Engineering Biodegradable and Biocompatible Bio-ionic Liquid Conjugated Hydrogels with Tunable Conductivity and Mechanical Properties, Sci Rep 7(1) (2017) 4345. [PubMed: 28659629]

[40]. Dvir T, Timko BP, Kohane DS, Langer R, Nanotechnological strategies for engineering complex tissues, Nat Nanotechnol 6(1) (2011) 13–22. [PubMed: 21151110]

[41]. Zhao G, Zhang X, Lu Tian J, Xu F, Recent Advances in Electrospun Nanofibrous Scaffolds for Cardiac Tissue Engineering, Advanced Functional Materials 25(36) (2015) 5726–5738.

[42]. Qazi TH, Rai R, Dippold D, Roether JE, Schubert DW, Rosellini E, Barbani N, Boccaccini AR, Development and characterization of novel electrically conductive PANI-PGS composites for cardiac tissue engineering applications, Acta Biomater 10(6) (2014) 2434–45. [PubMed: 24561709]

[43]. Martins AM, Eng G, Caridade SG, Mano JF, Reis RL, Vunjak-Novakovic G, Electrically conductive chitosan/carbon scaffolds for cardiac tissue engineering, Biomacromolecules 15(2) (2014) 635–43. [PubMed: 24417502]

[44]. Radhakrishnan J, Krishnan UM, Sethuraman S, Hydrogel based injectable scaffolds for cardiac tissue regeneration, Biotechnol Adv 32(2) (2014) 449–61. [PubMed: 24406815]

[45]. Liau B, Zhang D, Bursac N, Functional cardiac tissue engineering, Regen Med 7(2) (2012) 187–206. [PubMed: 22397609]

[46]. Ebrahimi AP, Mechanical properties of normal and diseased cerebrovascular system, J Vasc Interv Neurol 2(2) (2009) 155–62. [PubMed: 22518247]

[47]. Fioretta ES, Fledderus JO, Baaijens FP, Bouten CV, Influence of substrate stiffness on circulating progenitor cell fate, J Biomech 45(5) (2012) 736–44. [PubMed: 22169135]

[48]. Wang W, Zhang Y, Liu W, Bioinspired fabrication of high strength hydrogels from non-covalent interactions, Prog Polym Sci 71 (2017) 1–25.

[49]. Feng G, Djordjevic I, Mogal V, O'Rorke R, Pokholenko O, Steele TW, Elastic Light Tunable Tissue Adhesive Dendrimers, Macromol Biosci 16(7) (2016) 1072–82. [PubMed: 27061355]

[50]. Annabi N, Rana D, Shirzaei Sani E, Portillo-Lara R, Gifford JL, Fares MM, Mithieux SM, Weiss AS, Engineering a sprayable and elastic hydrogel adhesive with antimicrobial properties for wound healing, Biomaterials 139 (2017) 229–243. [PubMed: 28579065]

[51]. Cho E, Lee JS, Webb K, Formulation and characterization of poloxamine-based hydrogels as tissue sealants, Acta Biomater 8(6) (2012) 2223–32. [PubMed: 22406506]

[52]. Chen Q, Liang S, Thouas GA, Synthesis and characterisation of poly (glycerol sebacate)-co-lactic acid as surgical sealants, Soft Matter 7(14) (2011) 6484–6492.

[53]. Lang N, Pereira MJ, Lee Y, Friehs I, Vasilyev NV, Feins EN, Ablasser K, O'cearbhaill ED, Xu C, Fabozzo A, A blood-resistant surgical glue for minimally invasive repair of vessels and heart defects, Science translational medicine 6(218) (2014) 218ra6–218ra6.

[54]. Mooney DJ, Silva EA, Tissue engineering: a glue for biomaterials, Nat Mater 6(5) (2007) 327–8. [PubMed: 17471269]

[55]. Mehdizadeh M, Yang J, Design strategies and applications of tissue bioadhesives, Macromol Biosci 13(3) (2013) 271–88. [PubMed: 23225776]

[56]. Lawrence PG, Lapitsky Y, Ionically cross-linked poly(allylamine) as a stimulus- responsive underwater adhesive: ionic strength and pH effects, Langmuir 31(4) (2015) 1564–74. [PubMed: 25569307]

[57]. Zhu W, Chuah YJ, Wang DA, Bioadhesives for internal medical applications: A review, Acta Biomater 74 (2018) 1–16. [PubMed: 29684627]

[58]. Liang S, Zhang YY, Wang HB, Xu ZY, Chen JR, Bao R, Tan BY, Cui YL, Fan GW, Wang WX, Wang W, Liu WG, Paintable and Rapidly Bondable Conductive Hydrogels as Therapeutic Cardiac Patches, Advanced Materials 30(23) (2018).

[59]. Kazemzadeh-Narbat M, Rouwkema J, Annabi N, Cheng H, Ghaderi M, Cha BH, Aparnathi M, Khalilpour A, Byambaa B, Jabbari E, Tamayol A, Khademhosseini A, Engineering Photocrosslinkable Bicomponent Hydrogel Constructs for Creating 3D Vascularized Bone, Adv Healthc Mater 6(10) (2017).

[60]. Cochain C, Channon KM, Silvestre JS, Angiogenesis in the infarcted myocardium, Antioxid Redox Signal 18(9) (2013) 1100–13. [PubMed: 22870932]

[61]. Azevedo PS, Polegato BF, Minicucci MF, Paiva SA, Zornoff LA, Cardiac Remodeling: Concepts, Clinical Impact, Pathophysiological Mechanisms and Pharmacologic Treatment, Arq Bras Cardiol 106(1) (2016) 62–9. [PubMed: 26647721]

[62]. Liu Y, Lu J, Xu G, Wei J, Zhang Z, Li X, Tuning the conductivity and inner structure of electrospun fibers to promote cardiomyocyte elongation and synchronous beating, Mater Sci Eng C Mater Biol Appl 69 (2016) 865–74. [PubMed: 27612781]

[63]. Mathur A, Ma Z, Loskill P, Jeeawoody S, Healy KE, In vitro cardiac tissue models: Current status and future prospects, Adv Drug Deliv Rev 96 (2016) 203–13. [PubMed: 26428618]

[64]. Stoppel WL, Kaplan DL, Black LD 3rd, Electrical and mechanical stimulation of cardiac cells and tissue constructs, Adv Drug Deliv Rev 96 (2016) 135–55. [PubMed: 26232525]

[65]. McArthur L, Chilton L, Smith GL, Nicklin SA, Electrical consequences of cardiac myocyte: fibroblast coupling, Biochem Soc Trans 43(3) (2015) 513–8. [PubMed: 26009200]

[66]. Kohl P, Camelliti P, Burton FL, Smith GL, Electrical coupling of fibroblasts and myocytes: relevance for cardiac propagation, J Electrocardiol 38(4 Suppl) (2005) 45–50. [PubMed: 16226073]

[67]. Gaudesius G, Miragoli M, Thomas SP, Rohr S, Coupling of cardiac electrical activity over extended distances by fibroblasts of cardiac origin, Circulation research 93(5) (2003) 421–8. [PubMed: 12893743]

[68]. Struthers AD, Pathophysiology of heart failure following myocardial infarction, Heart 91 Suppl 2 (2005) ii14–6; discussion ii31, ii43–8. [PubMed: 15831601]

[69]. Zhao G, Zhang X, Lu TJ, Xu F, Recent Advances in Electrospun Nanofibrous Scaffolds for Cardiac Tissue Engineering, Advanced Functional Materials 25(36) (2015) 5726–5738.

[70]. Prabhakaran MP, Kai D, Ghasemi-Mobarakeh L, Ramakrishna S, Electrospun biocomposite nanofibrous patch for cardiac tissue engineering, Biomed Mater 6(5) (2011) 055001. [PubMed: 21813957]

[71]. Cui Z, Yang B, Li R-K, Application of Biomaterials in Cardiac Repair and Regeneration, Engineering 2(1) (2016) 141–148.

[72]. Capulli AK, MacQueen LA, Sheehy SP, Parker KK, Fibrous scaffolds for building hearts and heart parts, Adv Drug Deliv Rev 96 (2016) 83–102. [PubMed: 26656602]

[73]. Mauretti A, Spaans S, Bax NAM, Sahlgren C, Bouten CVC, Cardiac Progenitor Cells and the Interplay with Their Microenvironment, Stem Cells Int 2017 (2017) 7471582. [PubMed: 29075298]

[74]. Ebrahimi B, In vivo reprogramming for heart regeneration: A glance at efficiency, environmental impacts, challenges and future directions, J Mol Cell Cardiol 108 (2017) 61–72. [PubMed: 28502796]

[75]. Safari S, Malekvandfard F, Babashah S, Alizadehasl A, Sadeghizadeh M, Motavaf M, Mesenchymal stem cell-derived exosomes: A novel potential therapeutic avenue for cardiac regeneration, Cell Mol Biol (Noisy-le-grand) 62(7) (2016) 66–73. [PubMed: 27453275]

[76]. Pereira MJ, Carvalho IF, Karp JM, Ferreira LS, Sensing the cardiac environment: exploiting cues for regeneration, J Cardiovasc Transl Res 4(5) (2011) 616–30. [PubMed: 21735303]

[77]. Montgomery M, Ahadian S, Davenport Huyer L, Lo Rito M, Civitarese RA, Vanderlaan RD, Wu J, Reis LA, Momen A, Akbari S, Pahnke A, Li RK, Caldarone CA, Radisic M, Flexible shape-memory scaffold for minimally invasive delivery of functional tissues, Nat Mater 16(10) (2017) 1038–1046. [PubMed: 28805824]

[78]. Lang N, Pereira MJ, Lee Y, Friehs I, Vasilyev NV, Feins EN, Ablasser K, O'Cearbhaill ED, Xu C, Fabozzo A, Padera R, Wasserman S, Freudenthal F, Ferreira LS, Langer R, Karp JM, del Nido PJ, A blood-resistant surgical glue for minimally invasive repair of vessels and heart defects, Sci Transl Med 6(218) (2014) 218ra6.

[79]. Artzi N, Shazly T, Baker AB, Bon A, Edelman ER, Aldehyde-amine chemistry enables modulated biosealants with tissue-specific adhesion, Adv Mater 21(32–33) (2009) 3399–403. [PubMed: 20882504]

[80]. Nichol JW, Koshy ST, Bae H, Hwang CM, Yamanlar S, Khademhosseini A, Cell-laden microengineered gelatin methacrylate hydrogels, Biomaterials 31(21) (2010) 5536–44. [PubMed: 20417964]

[81]. Noshadi I, Walker BW, Portillo-Lara R, Shirzaei Sani E, Gomes N, Aziziyan MR, Annabi N, Engineering Biodegradable and Biocompatible Bio-ionic Liquid Conjugated Hydrogels with Tunable Conductivity and Mechanical Properties, Sci Rep-Uk 7(1) (2017) 4345.

[82]. Chandrasekharan A, Seong KY, Yim SG, Kim S, Seo S, Yoon J, Yang SY, In situ photocrosslinkable hyaluronic acid - based surgical glue with tunable mechanical properties and high adhesive strength, Journal of Polymer Science Part A: Polymer Chemistry (2018).

[83]. Kolk MV, Meyberg D, Deuse T, Tang-Quan KR, Robbins RC, Reichenspurner H, Schrepfer S, LAD-ligation: a murine model of myocardial infarction, J Vis Exp (32) (2009).

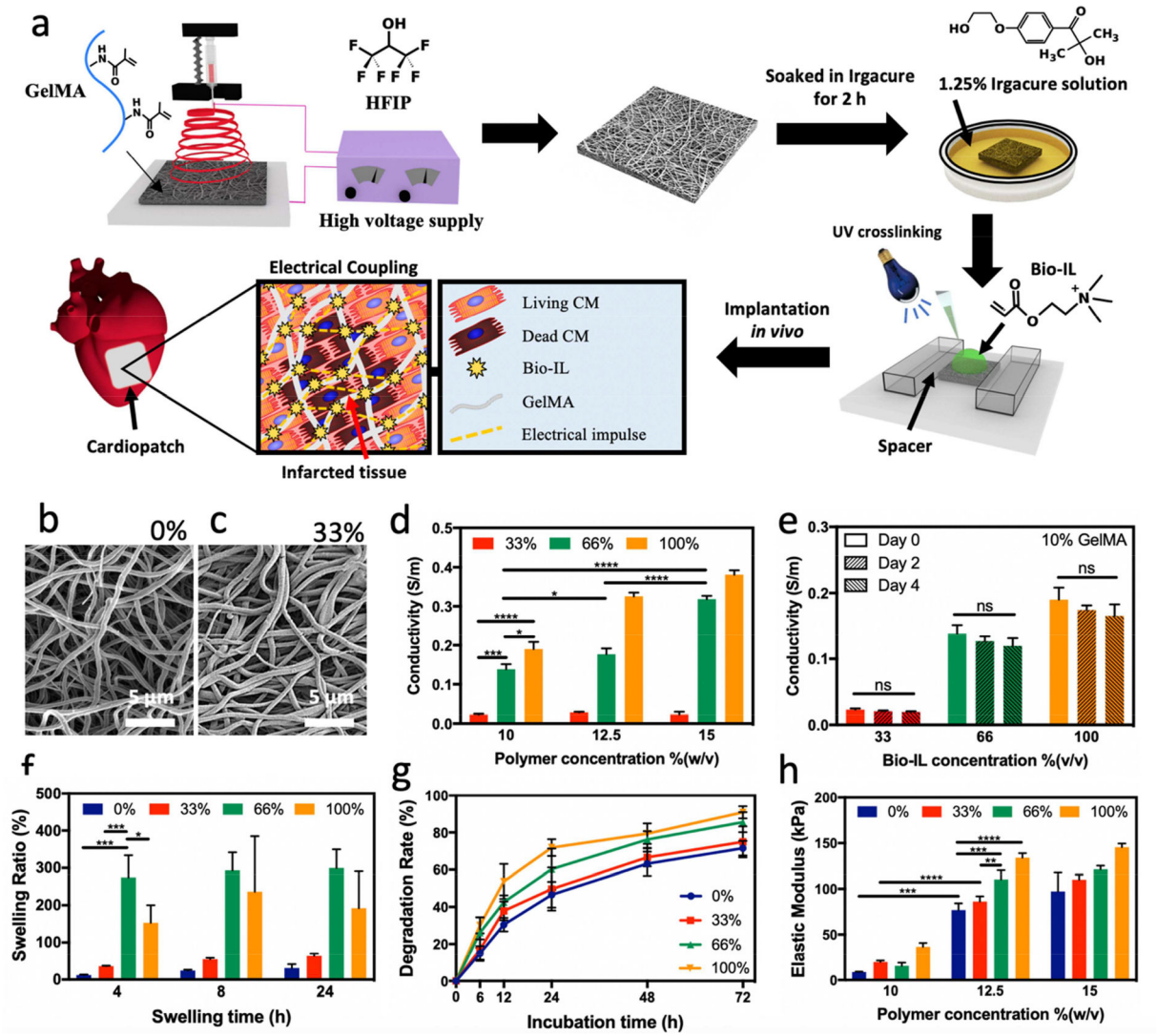

Figure 1. Synthesis and physical properties of electrospun GelMA/Bio-IL cardiopatches.

a) Schematic of the electrospinning of GelMA fibrous mats followed by soaking in Irgacure solution and Bio-IL addition prior to photocrosslinking with UV light for 5 min to form patches. Representative SEM images of patches formed by using 10% (w/v) GelMA with **b)** 0%, and **c)** 33% (v/v) Bio-IL. **d)** The electrical conductivity of cardiopatches fabricated with varying GelMA and Bio-IL concentrations, showing that the electrical conductivity of patches increased concomitantly when fabricated with higher concentrations of Bio-IL. **e)** The electroconductive properties of cardiac patches after incubation in DPBS at 37 °C for 2 and 4 days, which demonstrated that electrical conductivity did not decrease. **f)** Swelling ratio, **g)** degradation rate in collagenase type II solution over time, and h) elastic modulus of fabricated cardiopatches (for swelling ratio and degradation test 10% (w/v) GelMA was used). Error bars indicate standard error of the means, asterisks mark significance levels of $p < 0.05$ (*), $p < 0.01$ (**), and $p < 0.001$ (***).

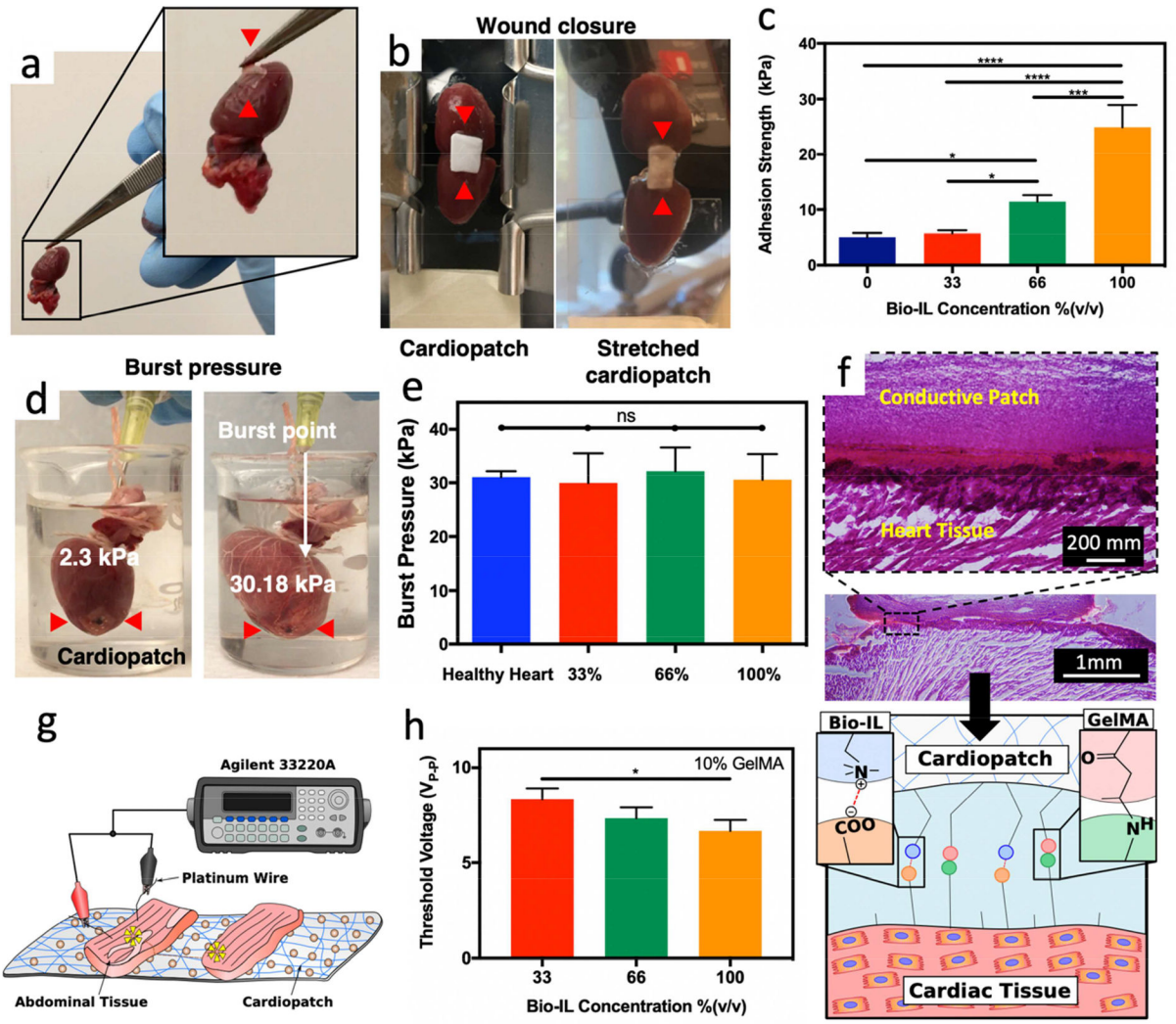

Figure 2. ***Ex vivo*** **Adhesive properties and electrical conductivity of GelMA/Bio-IL cardiopatches.**

a) Representative image of a GelMA/Bio-IL cardiopatch photocrosslinked on explanted rat heart demonstrating the high adhesion of the cardiopatch (red arrows) to cardiac tissues. **b)** Standard wound closure test using explanted rat heart as the biological substrate to test the adhesion strength of GelMA/Bio-IL cardiopatches. **c)** Quantification of the adhesion strength exhibited by cardiopatches fabricated with 10% (w/v) GelMA and varying concentrations of Bio-IL on explanted rat heart. Cardiopatches fabricated with higher concentrations of Bio-IL demonstrated higher adhesion strength to cardiac tissue. **d)** Representative images of GelMA/Bio-IL cardiopatch fabricated with 10% (w/v) GelMA and 66% (v/v) Bio-IL photocrosslinked on the defect site of an explanted rat heart to measure the burst pressure. **e)** Quantification of the burst pressure of GelMA/Bio-IL cardiopatches formed with varying concentrations of Bio-IL and photocrosslinked on the defect site of rat heart showed no significant difference when compared to the burst pressure of a healthy rat heart. **f)** H&E staining of cardiopatch-tissue interfaces. The tight interface indicates a strong bonding of the GelMA/Bio-IL cardiopatch to the murine myocardium. The schematic in

panel f showing the electrostatic forces between positively charged Bio-IL and negatively charged surface of cardiac muscle tissue and cells, as well as covalent bonds between methacrylate groups of GelMA and NH_2 functional groups in cardiac tissue. These two types of bonding led to strong adhesion. **g)** Schematic of *ex vivo* abdominal tissue placed adjacently on GelMA/Bio-IL cardiopatches fabricated with 10% (w/v) and varying concentrations of Bio-IL to determine the threshold voltage needed to stimulate both sections of abdominal tissue. **h)** Quantification of the threshold voltage of GelMA/Bio-IL cardiopatches significantly decreased for patches fabricated with 100% (v/v) Bio-IL compared to those fabricated with 33% (v/v) Bio-IL suggesting enhanced electrical properties with higher concentrations of Bio-IL. Error bars indicate standard error of the means, asterisks mark significance levels of $p < 0.05$ (*).

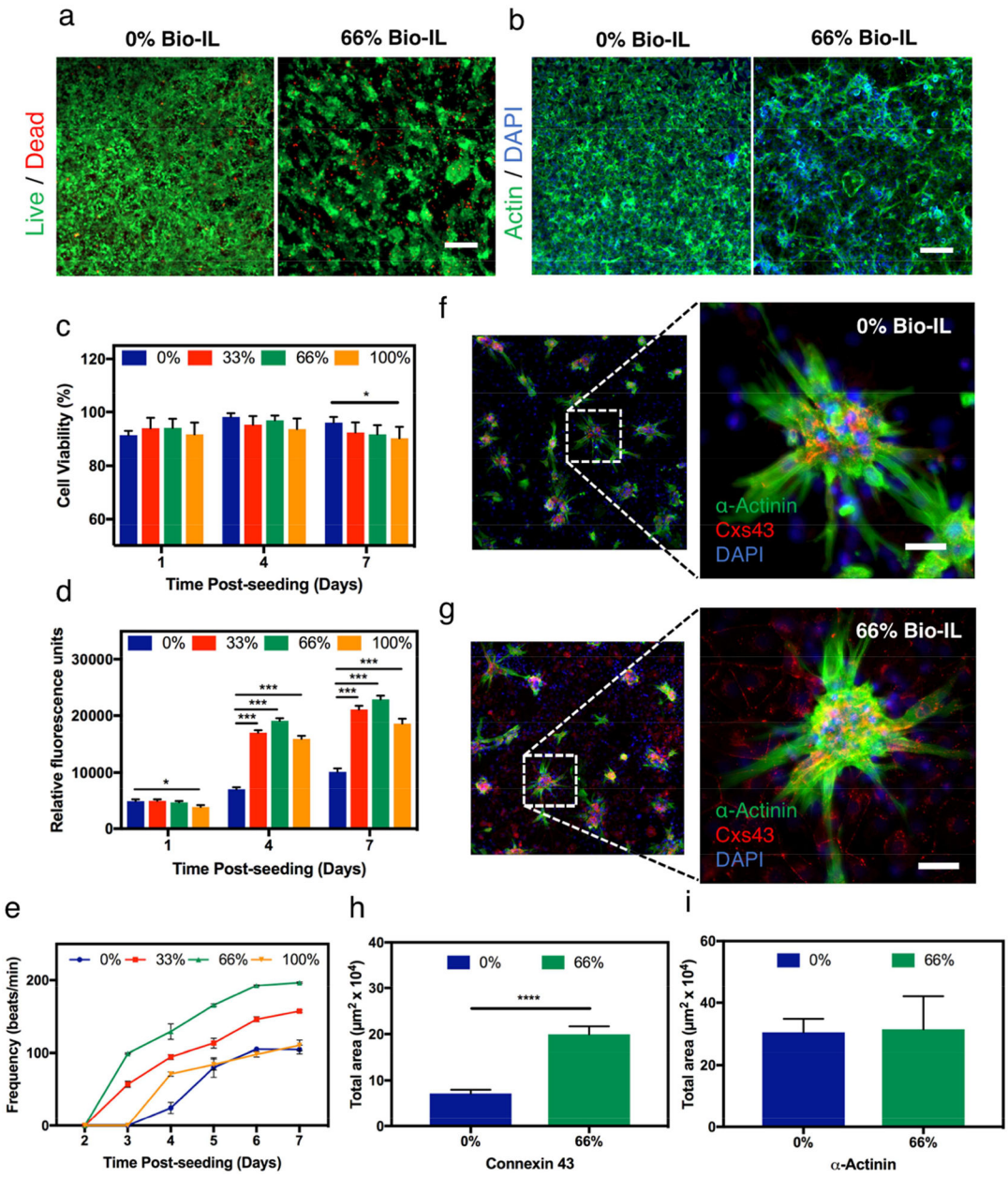

Figure 3. 2D co-cultures of CMs and CFs on GelMA/Bio-IL cardiopatches.

The *in vitro* cytocompatibility of the engineered cardiopatches was evaluated using 2D co-cultures of freshly isolated CMs and CFs (ratio 2:1) growing on cardiopatches fabricated with different concentrations of Bio-IL. **a)** Representative Live/Dead images of CMs/CFs growing on patches containing 0% and 66% (v/v) Bio-IL at day 7 post-seeding. **b)** Representative actin/DAPI images of CMs/CFs growing on patches fabricated with 0% and 66% (v/v) Bio-IL at day 7 post-seeding (Scale bar = 200 μm). Bar graphs showing the quantification of **c)** cell viability, and **d)** metabolic activity of 2D co-cultures of CMs/CFs at days 1, 4, and 7 post- seeding, growing on cardiopatches engineered with different concentrations of Bio-IL. **e)** Characterization of the beating frequency (beats/min) of CMs/CFs throughout 7 days of culture growing on cardiopatches fabricated with varying

concentrations of Bio-IL. Representative immunofluorescent images of CMs/CFs at day 7 post-seeding growing on the surface of patches containing **f)** 0%, and **g)** 66% (v/v) Bio-IL (green: sarcomeric α-actinin, red: connexin 43, blue: DAPI) (Scale bar = 50 μm). Quantification of the relative levels of expression (i.e., intensity of fluorescence) of **h)** connexin 43, and **i)** sarcomeric α-actinin in co-cultures of CMs/CFs on engineered patches at day 7 post-seeding.

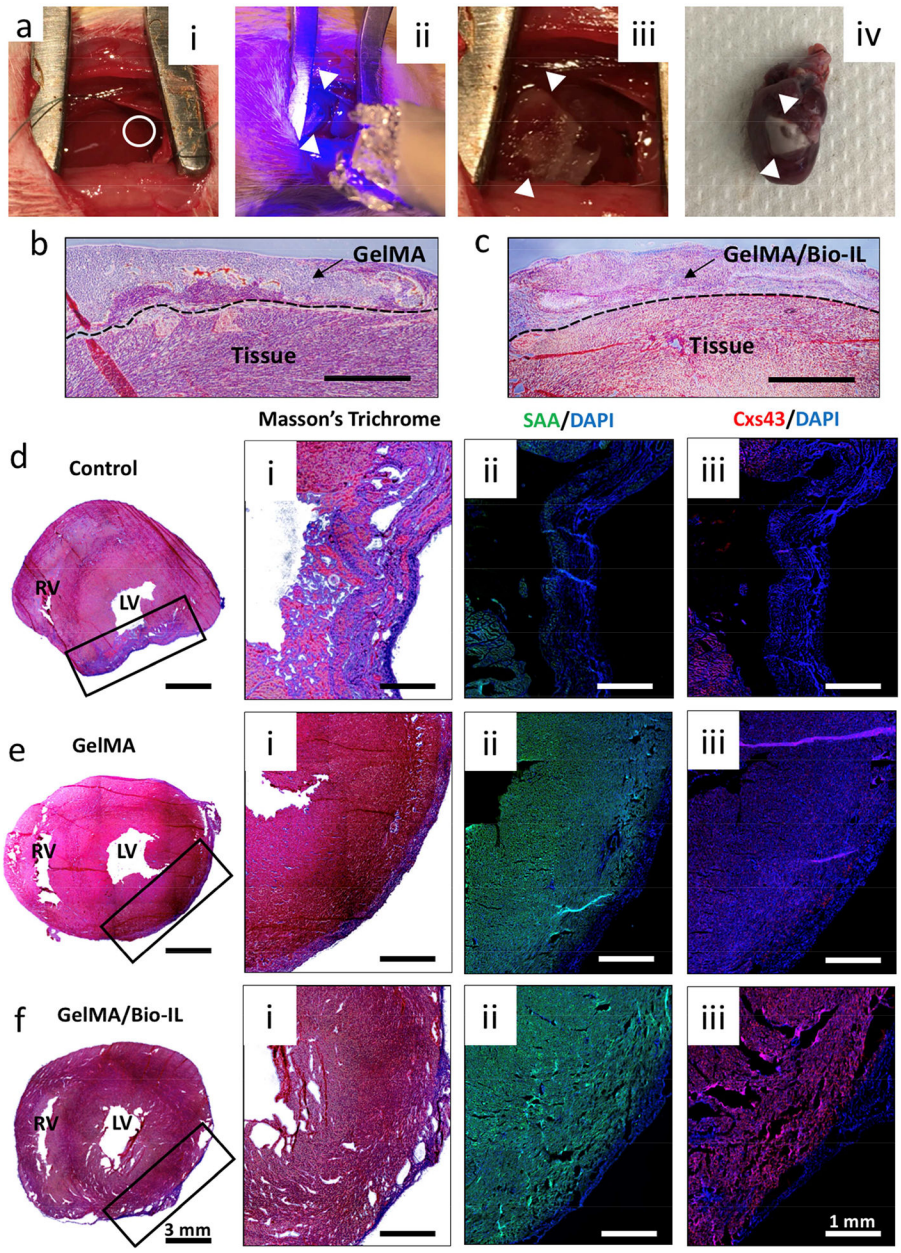

Figure 4. ***In vivo*** **evaluation of GelMA/Bio-IL cardiopatches using a murine model of MI.** Experimental MIs were induced via permanent ligation of the LAD coronary artery. **a)** Representative images showing: **a-i)** LAD ligation (white circle), **a-ii)** photocrosslinking of cardiopatches (white arrows) using UV light, **a-iii)** photocrosslinked cardiopatch on the heart, and **a-iv)** excised whole heart with cardiopatch distal to the site of LAD ligation after 21 days. Representative Masson's trichrome stained images from the interface between **b)** GelMA and **c)** GelMA/Bio-IL cardiopatches after 21 days (Scale bar = 400 μm). Representative Masson's trichrome and fluorescent stained images of excised hearts showing the location of the MIs in **di-iii)** untreated animal (sham), and animals treated with **ei-iii)** pristine GelMA patches, and **fi-iii)** GelMA/Bio-IL cardiopatches.